Dalton Transactions

Four-Component Relativistic ^{31}P NMR Calculations for *trans*-Platinum(II) Complexes: Importance of the Solvent and Dynamics in Spectral Simulations

Abril C. Castro,[a] Heike Fliegl,[b] Michele Cascella,[b] Trygve Helgaker,[b] Michal Repisky,[b] Stanislav Komorovsky,[c,d] María Ángeles Medrano,[e] Adoración G. Quiroga,[e] and Marcel Swart[a,f*]

Abstract. We report a combined experimental-theoretical study on the ^{31}P NMR chemical shift for a number of *trans*-platinum(II) complexes. Validity and reliability of the ^{31}P NMR chemical shift calculations are examined by comparing with the experimental data. A successful computational protocol for the accurate prediction of the ^{31}P NMR chemical shifts was established for *trans*-[PtCl$_2$(dma)PPh$_3$] (dma = dimethylamine) complex. The reliability of the computed values is shown to be critically dependent on the level of relativistic effects (two-component *vs.* four component), choice of density functional, dynamical averaging, and solvation effects. Snapshots from *ab initio* molecular dynamics simulations were used to identify those solvent molecules which show the largest interactions with the platinum complex, through inspection by the non-covalent interaction program. We observe satisfactory accuracy from the full four-component matrix Dirac-Kohn-Sham method (mDKS) based on the Dirac-Coulomb Hamiltonian, in conjunction with the KT2 density functional, and dynamical averaging with explicit solvent molecules.

Introduction

In the last decade, based on an improved understanding of the mechanism of action of anticancer platinum drugs,[1-9] *trans*-platinum complexes have demonstrated antitumor activity. Such emerging *non-classical* platinum complexes may lead to the development of better platinum drugs, in an attempt to minimize the severe side effects of cisplatin, one of the most important platinum complexes that exhibit antitumor activity.[10-11]

Crucial for establishing the mechanism of action of platinum complexes is their speciation in water solution, which has been studied in detail by several techniques.[12-16] Nuclear Magnetic Resonance (NMR) spectroscopy, in particular the multinuclear variants, is an useful tool for understanding the aquation of complexes under physiological conditions,[17-18] and very convenient to connect theory and experiment.[19] For platinum complexes containing aliphatic amines in a *trans* configuration, NMR studies demonstrated a direct relationship between the aquation process, the complexes' structure and their cytotoxicity.[20] Compounds with hydrophobic ligands like the phosphine PPh$_3$ and PMe$_2$Ph in a *trans* configuration to an aliphatic amine were shown to be very active.[21] However, there is no information about the aquation process of those compounds, not only because of their low solubility, but also because dimethyl sulfoxide (DMSO) overlaps with the aliphatic ^{1}H NMR signals making the detection of the species very difficult. In this regard, the use of ^{31}P NMR provides an alternative route for the characterization of the coordination sphere of these drugs.[21] Therefore, an accurate prediction of the ^{31}P chemical shifts is essential for assigning experimental spectra of these species in solution.

So far, the accurate prediction of heavy-metal nucleus NMR parameters poses challenges for quantum chemistry.[22-24] Calculated relativistic effects in the vicinity of a heavy metal are generally very sensitive to the character of metal-ligand bonding and the inclusion of environmental effects. Hence, specific difficulties arise when solvation is expected to be important, for which it is necessary to go beyond a static description and one needs to include the solvent dynamics. For instance, there is evidence demonstrating that conformational dynamics is essential for a proper determination of the NMR chemical shifts in various transition-metal complexes.[25] Examples of such assessments are the studies of Autschbach and co-workers for various Pt, Hg, and Pt-Te bonded complexes,[26-29] as well as the calculations performed by Bühl

a. *corresponding autor. Institut de Química Computacional i Catàlisi (IQCC), Departament de Química, Universitat de Girona, Campus Montilivi, 17003, Girona, Spain E-mail: marcel.swart@gmail.com*
b. *Hylleraas Centre for Quantum Molecular Sciences, Department of Chemistry, University of Oslo, P.O. Box 1033 Blindern, N-0315 Oslo, Norway*
c. *Hylleraas Centre for Quantum Molecular Sciences, Department of Chemistry, University of Tromsø/ The Arctic University of Norway, N-9037 Tromsø, Norway*
d. *Institute of Inorganic Chemistry, Slovak Academy of Sciences, Dúbravská cesta 9, SK-84536 Bratisla-va, Slovakia*
e. *Universidad Autónoma de Madrid, Dpto Química Inorgánica and Institute for Advanced Research in Chemical Sciences (IAdChem), Spain*
f. *ICREA, Pg. Lluís Companys 23, 08010 Barcelona, Spain*

Supporting information for this article is given via a link at the end of the document.

and co-workers for a number of Fe, Mn, V, and Co complexes.[30-32]

Although selected strategies have been employed before to treat these individual effects (*e.g.* molecular geometry, relativistic approximation, solvent), the reliable prediction and interpretation of NMR parameters still remains a major challenge in numerous transition-metal complexes. Intrigued by these considerations, we decided to carry out a combined experimental-theoretical study on the *trans*-[PtCl₂(dma)PPh₃] (dma = dimethylamine) complex **1** (Figure 1) and the speciation products in solution with the aim of establish a computational protocol for the reliable prediction of the ^{31}P NMR chemical shifts. Herein, complex **1** has been selected to address two important issues for the accurate prediction of the ^{31}P NMR employing DFT methods: (i) the validation of the relativistic DFT computational protocols (two-component *vs.* four component methods) and (ii) the role of the solvent effects and dynamic averaging on the calculated ^{31}P NMR (implicit *vs.* explicit solvent models).

Results and Discussion

Molecular structure and NMR studies in solution of trans-[PtCl2(dma)PPh3] (1). The *trans*-[PtCl₂(dma)PPh₃] complex **1** exhibits a square-planar geometry, slightly distorted around the platinum atom (Figure 1). Its hydrolysis involves a two-step reaction with the successive replacement of the two chloride ligands by water molecules from the solvent.[13,20] Complex **1** is soluble only in common organic solvents, in particular DMSO. Many attempts were performed to dissolve it and achieve the best conditions using the minimum amount of DMSO d_6. Ideal conditions for the study of the speciation products in solution were obtained using a sample of complex **1** in two different mixtures of solvents: (i) DMSO-d_6/H₂O(%D₂O) (90%/10%), and (ii) DMSO-d_6/H₂O(%D₂O)/acetone-d_6 (23% /66%/ 11%) (see details in the experimental section).

The detection of the speciation products monitored by ^{1}H NMR spectra becomes difficult since the methyl group from the dma ligand overlaps with the solvent signal (see Fig. S1a and S2a in the SI). Apart from monitoring by 1D-NMR, also 2D-NMR

experiments were used. In particular, the HSQC [^{1}H-^{13}C] NMR allows the detection of the dma's cross peak near the residual DMSO signal and to discard residual solvent coordination. Nevertheless, the signals corresponding to the coordinating species might fall inside the water suppression area and hence one should be cautious before discarding the coordination of DMSO. (see Fig. S1b and S2b in the SI).

In the ^{31}P NMR spectra, the initial complex **1** appears with a signal at 4.4 ppm (Figure 2). After 30 minutes, the solution with acetone shows two new signals around 16,5 and 18,1 ppm corresponding to two new species coexisting at pH 8; they may arise from water or DMSO coordination. After 4h, the solution shows a third new species at 31 ppm, coexisting with a species at 17,4 ppm (Figure 2). The species at 31 ppm may be due to a hydroxo complex, which has been reported before[33-34] in these reaction conditions for other platinum compounds. It is likely that in our case, the basic pH stabilizes hydroxo derivatives. At longer reaction times, the solution showed a different speciation (see Fig. S4 in the SI) and more complicated in the absence of acetone (figure S3 in the SI), meaning that over time the mixtures become more complex.

Relativistic effects to the ^{31}P NMR shielding constants and chemical shifts. As a first step, the experimental data have been compared with the results of relativistic DFT calculations based on *static* structures from geometry optimizations (thus neglecting specific solvent effects on the ^{31}P NMR chemical shift calculations). Since a mixture of water, DMSO and acetone was present in the experiments, each of which might be involved in the coordination to Pt, we considered all possibilities for the replacement of one or two chloride ligands by the three solvent molecules. Moreover, the insertion of one or two hydroxyl groups was also tested since hydroxide anions can coexist in the solution when the experiments are carried out at basic pH. The selected optimized structures are given in Figure S5 (see the SI).

For the chemical shift of 5d metals and heavy main-group elements, both scalar relativistic (SR) and spin-orbit (SO) relativistic effects play an important role.[35-36] To quantify these effects, two-component SR and SO relativistic zeroth-order regular approximation (ZORA)[37-41] calculations were performed
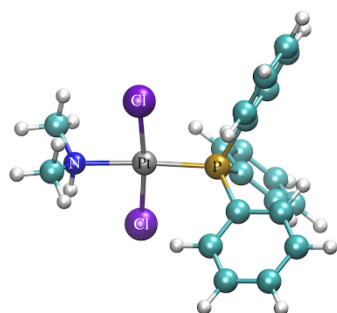
Figure 1. Structure of *trans*-[PtCl₂(dma)PPh₃] complex **1**.
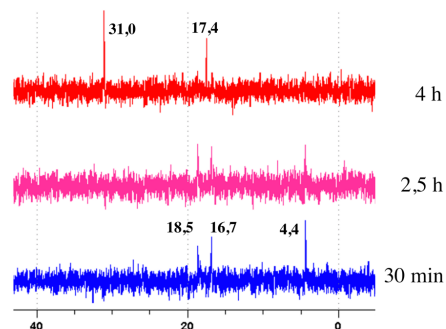
Figure 2. Progress of the complex in solution in conditions ii: DMSO d_6 (200 μl) and 300 μl of D₂O/H₂O/acetone (23%/66%/11%) at 30min (lower), 2.5h (middle), and 4h (top).

ARTICLE

for all the selected complexes using both PBE[42] and KT2[43] functionals. In addition, the basis set dependence was studied with the even-tempered (ET) STO-type (ET-pVQZ)[44] and the special STO-type (DZP, TZ2P, and QZ4P)[45] basis sets using the ADF program. Our results show clearly that the inclusion of SO effects is mandatory for both the shielding constants and the chemical shifts (see Tables S1 and S2 in the SI). Furthermore, there is only a small basis-set effect on the SO-ZORA relativistic corrections to the shielding constants, leading to changes of 1.4 ppm or less compared to the largest basis-set (QZ4P) results. In particular for complex **1**, the relative changes to the shielding constant are about 0.5-1.0 ppm. Furthermore, similar trends are found for the other selected complexes (see Tables S1 and S2, compounds 3-11 in the SI), even if the correction values do not always decrease from the smallest to the QZ4P basis set. The basis-set dependence becomes more important for the chemical shifts, ranging from 0.7 to 10.4 ppm. For complex **1**, the relative changes to the chemical shift have values of 2.6 ppm (DZP) and 0.7 ppm (ET-pVQZ) (see Tables S1 and S2 in the SI). For the relativistic corrections to the chemical shifts, it is, therefore, particularly important to use a large basis set.

In this study, theoretical approaches based on two- or four-component Hamiltonians are required as they include the relativistic corrections variationally from the start. Four-component relativistic calculations are generally more exact than two-component calculations, but also more demanding. However, in recent years, four-component calculations have become affordable for molecular systems of up to 200 atoms.[46-47] For cases when a four-component methodology is not available or too expensive, two-component SR and SO-ZORA calculations are an attractive alternative. For instance, it is known that the ZORA-DFT method performs very well for NMR observables and does not appear to be a source of large errors for computations of chemical shifts.[48] We have therefore studied relativistic effects to the ^{31}P shielding constants and chemical shifts using both two- and four-component relativistic corrections at the DFT level.

To calculate four-component relativistic corrections, we used the ReSpect (Relativistic Spectroscopy) program[49] and a full four-component matrix Dirac-Kohn-Sham method (mDKS) based on the Dirac-Coulomb Hamiltonian. In this case, the basis-set dependence was studied for the *trans*-[PtCl$_2$(dma)PPh$_3$] complex **1** using the mDKS/PBE level combined with the cvtz + vdz mixed basis set of Dyall,[50-52] as shown in Table S3 (see the SI). The accuracy on mDKS level of the ^{31}P shielding constant and chemical shift is not severely affected by using the smaller Dyall vdz basis set for the carbon and hydrogen atoms, justifying the present choice of basis sets as a good compromise between accuracy and computational cost.

A comparison of both SO-ZORA and mDKS relativistic corrections to the chemical shifts at the PBE and KT2 levels are shown in Table 1. If compared with the experimental signal of complex **1** (at 4.4 ppm), the calculated ^{31}P NMR shift values are notably upfield by up to 43.1 ppm. Among these methods, the

Table 1. Static ^{31}P NMR chemical shifts of the *trans*-platinum(II) complexes (in ppm) calculated with both SO-ZORA and mDKS relativistic corrections at the PBE and KT2 levels.

Complexes	mDKS / PBE[a]	ZORA / PBE[b]	mDKS / KT2[a]	ZORA / KT2[b]
1.[PtCl$_2$(dma)(PR$_3$)]	38.5	47.5	17.0	31.1
2. [PtCl(DMSO)(dma)(PR$_3$)]$^+$	31.5	39.4	9.9	23.4
3. [PtCl(H$_2$O)(dma)(PR$_3$)]$^+$	40.9	48.5	19.5	32.3
4. [PtCl(Acet)(dma)(PR$_3$)]$^+$	36.1	42.8	14.5	26.5
5. [Pt(DMSO)$_2$(dma)(PR$_3$)]$^{2+}$	38.5	44.5	17.2	28.8
6. [Pt(H$_2$O)$_2$(dma)(PR$_3$)]$^{2+}$	35.9	41.9	14.9	26.1
7. [Pt(Acet)$_2$(dma)(PR$_3$)]$^{2+}$	37.1	39.0	15.6	22.6
8. [Pt(DMSO)(H$_2$O)(dma)(PR$_3$)]$^{2+}$	38.5	43.6	17.4	28.0
9. [Pt(Acet)(DMSO)(dma)(PR$_3$)]$^{2+}$	38.7	42.9	17.3	26.6
10. [Pt(Acet)(H$_2$O)(dma)(PR$_3$)]$^{2+}$	36.0	39.0	14.7	22.6
11. [PtCl(OH)(dma)(PR$_3$)]	43.4	56.1	21.6	40.2
12. [Pt(OH)$_2$(dma)(PR$_3$)]	41.5	55.6	20.1	40.4

[a] calculated using the dyall_cvtz basis set. [b] calculated using the ET-pVQZ basis set. PR$_3$:PPh$_3$; Acet: Acetone

mDKS/KT2 level shows the best performance with a value of 17.0 ppm (Table 1, complex **1**). Furthermore, significant changes in chemical shift values and trends were revealed in the other complexes. Albeit differing from experiment, the four-component results must be considered as the most reliable since they represent the highest level of theory employed. Thus, the following sources of errors in the calculated ^{31}P NMR chemical shifts can be considered: (i) the limitations of the density functional (PBE, KT2), (ii) the use of correct and accurate structures, and (iii) the inclusion of environmental effects (no solvent effects have so far been included in the NMR calculations).

Dynamics and solvation effects on the ^{31}P NMR shielding constants. In the above calculations, the chemical shifts are not sufficiently well described using isolated structures. For this reason, we select the initial complex **1** to deeply investigate the role of the solvent effects. To determine the importance of the molecular movements (dynamics) and the effect of solvation, we performed AIMD simulations using the CP2K program package[64] where the phosphine (reference molecule) and complex **1** were surrounded by solvent molecules (water) and followed over time (see Supporting Information for details). From this trajectory, a total of 30 snapshots taken at regular intervals were used for obtaining dynamically averaged ^{31}P NMR nuclear shieldings.

Our first approach was to compute at these snapshots the shieldings for the solute alone (PH$_3$ or complex 1) with either SO-ZORA (gas-phase) or mDKS (gas-phase) and by including the COSMO dielectric continuum model[53-55] for solvation with SO-ZORA (Table 2). The SO-ZORA results show that the inclusion of the COSMO model leads only to minor changes, of up to 1.2-1.7 ppm for PH$_3$ and 1.2-1.4 ppm for complex 1. Once again, the importance of relativity becomes evident; the ^{31}P shielding values of PH$_3$ at the mDKS level are 21.9-23.1 ppm larger than the corresponding SO-ZORA values. This difference is even more pronounced for the shielding values of complex 1, with an

ARTICLE

Table 2. Dynamically calculated ^{31}P-NMR shielding (σ) constants of the PH_3 and *trans*-[PtCl$_2$(dma)PPh$_3$] complex calculated with selected methods and using the snapshots obtained from the AIMD simulations.

Method	Reference(PH$_3$) shielding(σ)	Pt complex shielding(σ)	Pt complex shift (δ)
SO-ZORA/PBE[a] (Gas-Phase)	554.2 ± 17.6	252.6 ± 9.2	38.4 ± 16.7
SO-ZORA/PBE[a] (COSMO)	552.5 ± 17.2	254.0 ± 9.0	35.3 ± 16.3
mDKS/PBE[b]	577.3 ± 16.5	285.3 ± 9.0	28.8 ± 16.0
SO-ZORA/KT2[a] (Gas-Phase)	577.6 ± 16.8	292.3 ± 8.9	22.1 ± 15.9
SO-ZORA/KT2[a] (COSMO)	576.4 ± 16.4	293.5 ± 8.7	19.7 ± 15.6
mDKS/KT2[b]	599.5 ± 18.0	330.7 ± 8.8	5.6 ± 16.7

[a] calculated using the ET-pVQZ basis set. [b] calculated using the dyall_cvtz basis set; c) from eq. 1.

increase of up to 32.7-38.4 ppm at the mDKS level. Furthermore, the large differences between the two density functionals here emerges, with KT2 giving nuclear shielding values that are 22-45 ppm larger than the corresponding PBE values. These differences persist in the chemical shifts (Table 2), where differences of 9.6-16.5 ppm are observed between SO-ZORA and mDKS, and 15.6-23.2 ppm between PBE and KT2.

Explicit treatment of the solvent. As second step in the treatment of the solvation process, the effect on the ^{31}P nuclear shielding of complex **1** was explored with varying numbers of explicit water molecules. The identification of which solvent molecules to include is, however, not straightforward; to avoid arbitrariness (visual inspection, chemical intuition), we resorted to the non-covalent interactions (NCI-plot) program.[56-57] This program visualizes the non-covalent interaction regions directly from the molecular density, indicating those areas where the interactions are strongest. In this manner, we arrived at a first coordination sphere consisting of three and five water molecules (see Figure 3, hydrogen-bonding interactions are indicated in blue and weaker dispersion interactions in green).
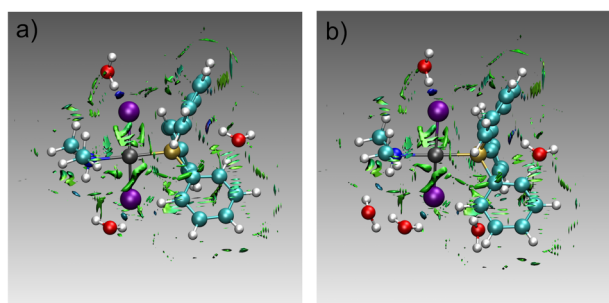
Figure 3. AIMD snapshots of complex **1** with (a) 3 and (b) 5 explicit water molecules, identified based on the non-covalent interaction regions (in blue/green) using the NCI program.

Although not quantitative, this method helps to identify which water molecules need to be taken into account in the present case. A comparison of the dynamically averaged ^{31}P NMR chemical shielding (σ) constants of complex **1** with and without explicit water molecules is given in Table S4 (see the Supporting Information). It is shown clearly that the effect of adding (three or five) solvent molecules is rather small (differences up to 0.4 ppm). This finding corroborates the results from the COSMO solvation model, which indicated that the effect of inclusion of solvents is minor compared to relativistic effects, dynamical averaging, and choice of density functional.

Discussion of the ^{31}P NMR Chemical Shift. Now that all effects have been explored systematically, a general comparison of the computational results can be made leading to the best estimates for the ^{31}P chemical shift of complex **1** (see Table 3). This takes into account how important the SO-ZORA and mDKS relativistic effects, choice of density functional (KT2 *vs.* PBE), dynamical averaging, and solvation effects are.

The first thing to notice is the importance of including dynamical averaging when calculating ^{31}P NMR chemical shifts. This can be understood both in terms of vibrational averaging over the degrees of freedom of the molecule (at room temperature), and in terms of the indirect effect induced by the presence of the solvent molecules in the AIMD simulations. Although the direct effect of the solvent molecules on the nuclear shielding is small (*vide supra*), their presence has an effect on the geometry of the solute, thereby limiting the space available for exploration by the solute (steric effects), and enhancing the favorable weak (*e.g.*, hydrogen-bonding, dispersion) interactions. For this reason, the effect of dynamical averaging goes in opposite directions for the phosphine reference molecule and complex **1** (see Table 3); whereas the nuclear shielding decreases for the former upon dynamical averaging (up to -7.7 ppm), it increases for the latter (up to +3.7 ppm). Obviously, this directly affects the chemical shift, which decreases after dynamical averaging by 9.0-11.4 ppm. Thus, it is of crucial importance to obtain a correct description of the reference compound, which appears to be very dependent on the underlying choice of density functional, and the relativistic treatment.

Furthermore, the addition of explicit solvent molecules enhances this effect. The shielding constants of the Pt complex get further increased at the SO-ZORA level but remain almost constant at the mDKS level. Thus, inclusion of explicit solvent molecules needs to be carefully monitored to ensure that convergence upon inclusion of explicit water molecules has been achieved.

Our findings are summarized in Figure 4, which shows that the inclusion of dynamic effects is of crucial importance for an accurate description of ^{31}P NMR chemical shifts. The calculated results closest to experiment are always obtained with the KT2 functional; this should not come as a surprise since it was designed[43] for describing well the potential in the nuclear region and hence was reported to work well for NMR shieldings.[58-59]

Dalton Transactions ARTICLE

Table 3. Static and dynamic ³¹P NMR chemical shifts[a] of complex **1**.

		Reference (PH₃) Shielding (σ)	Complex Shielding (σ)	Shift (δ)[c]
Experimental shift value		---	---	4.4
SO-ZORA/PBE[b]				
Static- Gas phase	Isolated complex	560.9	250.2	47.5
Static- COSMO	Isolated complex	559.1	251.4	44.5
Static- Gas phase	Explicit 3 water molecules	560.9	257.4	40.3
Dynamic	Isolated complex	554.2± 17.6	252.6 ± 9.2	38.4
Dynamic	Explicit 3 water molecules	554.2 ± 17.6	256.0 ± 9.5	35.0
Dynamic	Explicit 5 water molecules	554.2 ± 17.6	256.9 ± 9.6	34.1
SO-ZORA/KT2[b]				
Static- Gas phase	Isolated complex	584.0	289.7	31.1
Static- COSMO	Isolated complex	582.7	290.8	28.7
Static- Gas phase	Explicit 3 water molecules	584.0	297.1	23.7
Dynamic	Isolated complex	577.6 ± 16.8	292.3 ± 8.9	22.1
Dynamic	Explicit 3 water molecules	577.6 ± 16.8	295.8 ± 9.3	18.6
Dynamic	Explicit 5 water molecules	577.6 ± 16.8	296.7 ± 9.3	17.7
mDKS/PBE[c]				
Static- Gas phase	Isolated complex	583.8	282.1	38.5
Static- Gas phase	Explicit 3 water molecules	583.8	284.7	35.9
Dynamic	Isolated complex	577.3 ± 16.5	285.3 ± 9.0	28.8
Dynamic	Explicit 3 water molecules	577.3 ± 16.5	285.5 ± 8.9	28.6
Dynamic	Explicit 5 water molecules	577.3 ± 16.5	285.7 ± 8.9	28.4
mDKS/KT2[c]				
Static- Gas phase	Isolated complex	607.2	327.0	17.0
Static- Gas phase	Explicit 3 water molecules	607.2	329.2	14.8
Dynamic	Isolated complex	599.5 ± 18.0	330.7 ± 8.8	5.6
Dynamic	Explicit 3 water molecules	599.5 ± 18.0	330.8 ± 8.7	5.5
Dynamic	Explicit 5 water molecules	599.5 ± 18.0	330.9 ± 8.7	5.4

[a] correction value of -263.2 ppm, from eq. 1; b) calculated using the ET-pVQZ basis set, c) calculated using the dyall_cvtz basis set.
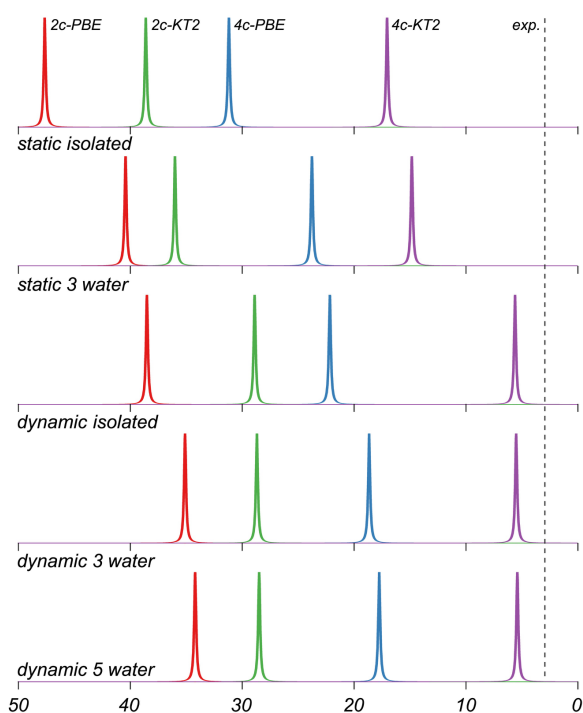
Figure 4. Computed ³¹P NMR chemical shifts of complex **1** calculated using SO-ZORA (2c) and mDKS (4c) relativistic corrections at the PBE and KT2 levels. The experimental value is indicated by a dashed line.

[69] Furthermore, the increased accuracy of four-component mDKS over two-component SO-ZORA was to be expected. Hence, the best match as compared to experiment (difference of only 1.0 ppm) has been obtained using the four-component mDKS level with KT2. It is somewhat surprising that inclusion of explicit solvent molecules has a somewhat more pronounced effect at the SO-ZORA than at the four-component mDKS level.

Conclusions

We have examined the reliability of different levels of theory for the calculation of ³¹P NMR chemical shifts in a series of *trans*-platinum(II) complexes. We have shown that the calculation of the ³¹P chemical shifts for these compounds remains a challenge for computational chemistry and that no simple protocol can be established for such studies. The identification of the species observed experimentally failed when *static* ³¹P NMR calculations using both two- and four-component relativistic corrections were used. Although limited in scope, the computational protocol carried out in this work allowed the accurate identification of complex **1**, which would otherwise be inaccessible using standard protocols.

In particular, our study revealed that it is necessary to perform a comparatively high-level modeling of solvation on both the

probe and the reference molecule. Solvation influences the ^{31}P chemical shift via structural parameters, dynamics, and electronic solvent-solute interactions. The latter cannot be properly modeled with a continuum model, although such a model is instrumental for describing bulk solvent effects. We have shown that ^{31}P chemical shifts may be obtained in reasonable agreement with experimental values if the solvent-solute interactions are modeled at a high level. The choice of the reference molecule and the relativistic effects are of crucial importance and are the main factors that influence the quality in the ^{31}P NMR chemical shift calculations.

Based on the results obtained in this study we recommend to (i) include dynamic effects and (ii) use the four-component mDKS method together with the KT2 functional for an accurate description of ^{31}P NMR chemical shifts for the Pt compounds investigated herein. An investigation on the speciation products in solution using the computational protocol proposed here is currently underway.

Experimental Section

Solution state NMR experiments

The *in vitro* studies performed in cancer cells[60] using 1% of DMSO in water solutions showed activity in the nanomolar range, hence only a low concentration of the compound is required for an effective introduction of the drug in the system. However, the experimental conditions for the NMR studies dictate a higher concentration than nanomolar. Furthermore, after several attempts to determine the minimum amount of DMSO d_6 needed, the optimal conditions were achieved (ca. 35% (**I**) and 25% (**II**)). Moreover, we tried to assay the solution experiments with another solvent (acetone), which always led to a milky appearance with water. Therefore, DMSO needed to be included again.

The *trans*-Pt(dma)(PPh$_3$)Cl$_2$ (**1**) was prepared following a procedure previously reported,[60] and the sample used to study its behavior in solution were prepared by mixing 2 mg of complex **1** in a mixture of deuterated solvents to a final volume of 0.5 mL in an NMR tube. Two different solutions were used in the study, with a final content of:

DMSO d_6 (200μl) and 300μl of D_2O/H_2O (90%/10%)

DMSO d_6 (200μl) and 300μl of D_2O/H_2O/acetone-d_6 (23%/66%/11%).

The time preparation of the fresh spectra (t=0) has not been taken into consideration, and the procedure takes at least 15 minutes, after which the aquation process has already begun. All the deuterated solvents and solutions were previously warmed up to 37 degrees. The sample (a) was initially dissolved in 50μL of DMSO d_6, then a mixture containing 150μl of DMSO d_6 and 150μl of D_2O/H_2O was prepared and slowly added to the initial solution with stirring. The final 150μl of D_2O/H_2O were added and the tube was maintained at 37ºC under slight stirring during the entire experiment (24h) using a thermoshaker. Sample (b) was performed similarly using a slow addition of a mixture (100μl of DMSO d_6 with 150μl of D_2O/H_2O/acetone d_6) over 50μl of complex **1** in DMSO.

NMR spectra were recorded on a Bruker Avance III-HD NANOBAY (300 MHz) spectrometer at room temperature (25 ºC) at Interdepartmental Investigation Service (SIdI) of the Universidad Autónoma de Madrid, using H_3PO_4 as internal reference.

Computational Details

All electronic-structure calculations were performed with density functional theory (DFT), using the Amsterdam Density Functional (ADF),[61-62] QUILD,[63] ReSpect (Relativistic Spectroscopy)[49] and CP2K[64] programs. The dispersion-corrected PBE[42] and KT2 functional[43] were used, with scalar (SR) and spin-orbit (SO) relativistic effects included at the two-component level using the zeroth-order regular approximation Hamiltonian (ZORA),[38,40] and the full four-component matrix Dirac-Kohn-Sham method (mDKS) based on the Dirac-Coulomb Hamiltonian. All the shielding constants were obtained with the GIAO method.[65]

Solvation effects were taken into account both through a dielectric continuum model (COSMO)[53-55] and by including explicit solvent molecules in molecular dynamics simulations. To keep the four-component relativistic NMR calculations feasible and be able to take a larger number of snapshots from the MD simulations, we used the NCI-plot program[56-57] to identify the most relevant water molecules to take into account for the solvent-complex interactions (see the Supporting Information for full details).

All calculated ^{31}P shielding constants σ_{calc} were converted to ^{31}P NMR chemical shifts δ_{calc} (ppm, 85% aqueous solution of H_3PO_4) using Eq. (1) as suggested by Lantto *et al.*[66] (it was -266.1 ppm in Ref. [67-68]):

$$\delta_{calc} = \sigma_{calc}(PH_3) - \sigma_{calc} - 263.2 \text{ ppm} \qquad (1)$$

where $\sigma_{calc}(PH_3)$ is the absolute ^{31}P NMR shielding constant of phosphine (PH_3) calculated at the same level of theory and with the same basis set.

Conflicts of interest

There are no conflicts to declare.

Acknowledgements

Notes and references

1   T. W. Hambley, *Coord. Chem. Rev.*, 1997, **166**, 181-223.
2   E. R. Jamieson, S. J. Lippard, *Chem. Rev.*, 1999, **99** (9), 2467-2498.
3   J. Reedijk, *Chem. Commun.*, 1996, (7), 801-806.
4   T. C. Johnstone, K. Suntharalingam, S. J. Lippard, *Chem. Rev.*, 2016, **116** (5), 3436-3486.
5   J. S. Butler, J. A. Woods, N. J. Farrer, M. E. Newton, P. J. Sadler, *J. Am. Chem. Soc.*, 2012, **134**, 16508-16511.
6   T. C. Johnstone, S. J. Lippard, *J. Am. Chem. Soc.*, 2014, **136**, 2126-2134.

Dalton Transactions

7   V. Venkatesh, N. K. Mishra, I. Romero-Canelón, R. R. Vernooij, H. Shi, J. P. C. Coverdale, A. Habtemariam, S. Verma, P. J. Sadler, *J. Am. Chem. Soc.*, 2017, **139**, 5656-5659.

8   V. Ramu, S. Gautam, A. Garai, P. Kondaiah, A. R. Chakravarty, *Inorg. Chem.*, 2018, **57**, 1717-1726.

9   T. R. Schulte, J. J. Holstein, L. Krause, R. Michel, D. Stalke, E. Sakuda, K. Umakoshi, G. Longhi, S. Abbate, G. H. Clever, *J. Am. Chem. Soc.*, 2017, **139**, 6863-6866.

10   1D. Lebwohl, R. Canetta, *Eur. J. Cancer*, 1998, **34** (10), 1522-1534.

11   P. J. O'Dwyer, J. P. Stevenson, *Clinical status of cisplatin, carboplatin, and other platinum-based antitumor drugs, Cisplatin: Chemistry and Biochemistry of a Leading Anticancer Drug*. 1999.

12   R. B. Martin, *Cisplatin: Chemistry and Biochemistry of a Leading Anticancer Drug.*, Wiley-VCH, Zürich, 1999.

13   S. J. Berners-Price, T. A. Frenkiel, U. Frey, J. D. Ranford, P. J. Sadler, *J. Chem. Soc., Chem. Commun.*, 1992, (10), 789-791.

14   L. Cubo, D. S. Thomas, J. Zhang, A. G. Quiroga, C. Navarro-Ranninger, S. J. Berners-Price, *Inorg. Chim. Acta*, 2009, **362** (3), 1022-1026.

15   A. A. Vernekar, G. Berger, A. E. Czapar, F. A. Veliz, D. I. Wang, N. F. Steinmetz, S. J. Lippard, *J. Am. Chem. Soc.*, 2018, **140**, 4279-4287.

16   A. C. Samuels, C. A. Boele, K. T. Bennett, S. B. Clark, N. A. Wall, A. E. Clark, *Inorg. Chem.*, 2014, **53**, 12315-12322.

17   S. J. Berners-Price, L. Ronconi, P. J. Sadler, *Prog. Nucl. Magn. Reson. Spectrosc.*, 2006, **49** (1), 65-98.

18   A. G. Quiroga, *J. Inorg. Biochem.*, 2012, **114**, 106-112.

19   A. C. Castro, M. Swart, C. F. Guerra, *Phys. Chem. Chem. Phys.*, 2017, **19** (21), 13496-13502.

20   L. Cubo, A. G. Quiroga, J. Zhang, D. S. Thomas, A. Carnero, C. Navarro-Ranninger, S. J. Berners-Price, *Dalton Trans.*, 2009, (18), 3457-3466.

21   Francisco J. Ramos-Lima, Adoración G. Quiroga, José M. Pérez, M. Font-Bardía, X. Solans, C. Navarro-Ranninger, *Eur. J. Inorg. Chem.*, 2003, **2003** (8), 1591-1598.

22   J. Autschbach, Calculating NMR Chemical Shifts and J-Couplings for Heavy Element Compounds. In *Enc. Anal. Chem.*, John Wiley & Sons, Ltd: 2006.

23   M. Bühl, T. van Mourik, *WIREs Comput. Mol. Sci.*, 2011, **1** (4), 634-647.

24   C. J. Jameson, Calculation of Nuclear Magnetic Resonance Parameters. In *Enc. Anal. Chem.*, John Wiley & Sons, Ltd: 2006.

25   *Calculation of NMR and EPR Parameters*. M. B. Eds. M. Kaupp, and V. G. Malkin, Wiley-VCH, Verlag GmbH & Co. KGaA, 2004.

26   L. A. Truflandier, K. Sutter, J. Autschbach, *Inorg. Chem.*, 2011, **50** (5), 1723-1732.

27   J. Autschbach, T. Ziegler, *J. Am. Chem. Soc.*, 2001, **123** (14), 3341-3349.

28   J. Autschbach, T. Ziegler, *J. Am. Chem. Soc.*, 2001, **123** (22), 5320-5324.

29   B. Le Guennic, K. Matsumoto, J. Autschbach, *Magn. Reson. Chem.*, 2004, **42** (S1), S99-S116.

30   M. Bühl, F. T. Mauschick, F. Terstegen, B. Wrackmeyer, *Angew. Chem. Int. Ed.*, 2002, **41** (13), 2312-2315.

31   M. Bühl, R. Schurhammer, P. Imhof, *J. Am. Chem. Soc.*, 2004, **126** (10), 3310-3320.

32   M. Bühl, S. Grigoleit, H. Kabrede, F. T. Mauschick, *Chem. Eur. J.*, 2005, **12** (2), 477-488.

33   E. Costa, M. Murray, P. G. Pringle, M. B. Smith, *Inorg. Chim. Acta*, 1993, **213** (1), 25-28.

34   B. Longato, L. Pasquato, A. Mucci, L. Schenetti, *Eur. J. Inorg. Chem.*, 2002, **2003** (1), 128-137.

35   J. Vícha, J. Novotny, M. Straka, M. Repisky, K. Ruud, S. Komorovsky, R. Marek, *Phys. Chem. Chem. Phys.*, 2015, **17** (38), 24944-24955.

36   J. Novotný, J. Vícha, P. L. Bora, M. Repisky, M. Straka, S. Komorovsky, R. Marek, *J. Chem. Theory Comput.*, 2017, **13** (8), 3586-3601.

37   E. van Lenthe, A. Ehlers, E.-J. Baerends, *J. Chem. Phys.*, 1999, **110** (18), 8943-8953.

38   E. van Lenthe, E. J. Baerends, J. G. Snijders, *J. Chem. Phys.*, 1993, **99** (6), 4597-4610.

39   E. van Lenthe, E. J. Baerends, J. G. Snijders, *J. Chem. Phys.*, 1994, **101** (11), 9783-9792.

40   E. van Lenthe, J. G. Snijders, E. J. Baerends, *J. Chem. Phys.*, 1996, **105** (15), 6505-6516.

41   E. van Lenthe, R. van Leeuwen, E. J. Baerends, J. G. Snijders, *Int. J. Quantum Chem*, 1996, **57** (3), 281-293.

42   J. P. Perdew, K. Burke, M. Ernzerhof, *Phys. Rev. Lett.*, 1996, **77** (18), 3865-3868.

43   T. W. Keal, D. J. Tozer, *J. Chem. Phys.*, 2003, **119** (6), 3015-3024.

44   D. P. Chong, E. Van Lenthe, S. Van Gisbergen, E. J. Baerends, *J. Comput. Chem.*, 2004, **25** (8), 1030-1036.

45   E. van Lenthe, E. J. Baerends, *J. Comput. Chem.*, 2003, **24** (9), 1142-1156.

46   P. Hrobárik, V. Hrobáriková, F. Meier, M. Repiský, S. Komorovský, M. Kaupp, *J. Phys. Chem. A*, 2011, **115** (22), 5654-5659.

47   J. Vícha, R. Marek, M. Straka, *Inorg. Chem.*, 2016, **55** (4), 1770-1781.

48   J. Autschbach, *Theor. Chem. Acc.*, 2004, **112** (1), 52-57.

49   Repisky, M.; Komorovský, S.; Malkin, V. G.; Malkina, O. L.; Kaupp, M.; Ruud, K.; with contributions from Bast, R.; Ekström, U.; Kadek, M.; Knecht, S.; Konecny, L.; Malkin, E.; Malkin-Ondik, I. *ReSpect, Relativistic Spectroscopy DFT program*, ReSpect, Relativistic Spectroscopy DFT program (see http://www.respectprogram.org), version 4.0.0; 2016.

50   K. G. Dyall, unpublished; available from web site, http://dirac.chem.sdu.dk/.

51   K. G. Dyall, *Theor. Chem. Acc.*, 2004, **112** (5), 403-409.

52   A. S. P. Gomes, K. G. Dyall, L. Visscher, *Theor. Chem. Acc.*, 2010, **127** (4), 369-381.

53   A. Klamt, G. Schuurmann, *J. Chem. Soc., Perkin Trans. 2*, 1993, (5), 799-805.

54   A. Klamt, *J. Phys. Chem.*, 1996, **100** (9), 3349-3353.

55   C. C. Pye, T. Ziegler, *Theor. Chem. Acc.*, 1999, **101** (6), 396-408.

56   E. R. Johnson, S. Keinan, P. Mori-Sánchez, J. Contreras-García, A. J. Cohen, W. Yang, *J. Am. Chem. Soc.*, 2010, **132** (18), 6498-6506.

57   J. Contreras-García, E. R. Johnson, S. Keinan, R. Chaudret, J.-P. Piquemal, D. N. Beratan, W. Yang, *J. Chem. Theory Comput.*, 2011, **7** (3), 625-632.

58   L. Armangué, M. Solà, M. Swart, *J. Phys. Chem. A*, 2011, **115** (7), 1250-1256.

59   A. M. Teale, O. B. Lutnæs, T. Helgaker, D. J. Tozer, J. Gauss, *J. Chem. Phys.*, 2013, **138** (2), 024111.

60   F. J. Ramos-Lima, A. G. Quiroga, B. García-Serrelde, F. Blanco, A. Carnero, C. Navarro-Ranninger, *J. Med. Chem.*, 2007, **50** (9), 2194-2199.

61   E. J. Baerends, T. Ziegler, A. J. Atkins, J. Autschbach, D. Bashford, A. Bérces, F. M. Bickelhaupt, C. Bo, P. M. Boerrigter, L. Cavallo, D. P. Chong, D. V. Chulhai, L. Deng, R. M. Dickson, J. M. Dieterich, D. E. Ellis, M. v. Faassen, L. Fan, T. H. Fischer, C. Fonseca Guerra, M. Franchini, A. Ghysels, A. Giammona, S. J. A. van Gisbergen, A. W. Götz, J. A. Groeneveld, O. V. Gritsenko, M. Grüning, S. Gusarov, F. E. Harris, T. Heine, P. van den Hoek, C. R. Jacob, H. Jacobsen, L. Jensen, J. W. Kaminski, G. van Kessel, F. Kootstra, A. Kovalenko, M. V. Krykunov, E. van Lenthe, D. A. McCormack, A. Michalak, M. Mitoraj, S. M. Morton, J. Neugebauer, V. P. Nicu, L. Noodleman, V. P. Osinga, S. Patchkovskii, M. Pavanello, C. A. Peeples, P. H. T. Philipsen, D. Post, C. C. Pye, W. Ravenek, J. I. Rodríguez, P. Ros, R. Rüger,

P. R. T. Schipper, H. van Schoot, G. Schreckenbach, J. S. Seldenthuis, M. Seth, J. G. Snijders, M. Solà, M. Swart, D. Swerhone, G. te Velde, P. Vernooijs, L. Versluis, L. Visscher, O. Visser, F. Wang, T. A. Wesolowski, E. M. van Wezenbeek, G. Wiesenekker, S. K. Wolff, T. K. Woo, A. L. Yakovlev *ADF2016*, ADF2016.01; SCM, Theoretical Chemistry, Vrije Universiteit: Amsterdam, 2016.

62 G. te Velde, F. M. Bickelhaupt, E. J. Baerends, C. Fonseca Guerra, S. J. A. van Gisbergen, J. G. Snijders, T. Ziegler, *J. Comput. Chem.*, 2001, **22** (9), 931-967.

63 M. Swart, F. M. Bickelhaupt, *J. Comput. Chem.*, 2008, **29** (5), 724-734.

64 CP2K Developers Group, URL. http://www.cp2k.org/ (accessed Sep 2, 2016).

65 R. Ditchfield, *Mol. Phys.*, 1974, **27** (4), 789-807.

66 P. Lantto, K. Jackowski, W. Makulski, M. Olejniczak, M. Jaszuński, *J. Phys. Chem. A*, 2011, **115** (38), 10617-10623.

67 C. J. Jameson, A. De Dios, A. Keith Jameson, *Chem. Phys. Lett.*, 1990, **167** (6), 575-582.

68 C. van Wüllen, *Phys. Chem. Chem. Phys.*, 2000, **2** (10), 2137-2144.

69 Rusakov YY, Rusakova IL, Krivdin LB. Relativistic heavy atom effect on the ^{31}P NMR parameters of phosphine chalcogenides. Part 1. Chemical shifts. Magn Reson Chem. 2018;56: 1061–1073. https://doi.org/10.1002/mrc.4752